Article:

Guilbaud, R, Poulton, SW orcid.org/0000-0001-7621-189X, Thompson, J et al. (5 more authors) (2020) Phosphorus-limited conditions in the early Neoproterozoic ocean maintained low levels of atmospheric oxygen. Nature Geoscience. ISSN 1752-0894

https://doi.org/10.1038/s41561-020-0548-7

SUPPLEMENTARY INFORMATION

'Phosphorus-limited conditions in the early Neoproterozoic ocean maintained low levels of atmospheric oxygen'

Guilbaud et al.

The Supplementary Information includes details on geological setting, P speciation and C isotope quality checks, a compilation of organic C through time (from ref. 1) and C/P ratios in the Phanerozoic, a geological and redox framework for the complementary data from the Taoudeni and the Animikie Basins, and key assumptions of the Daines et al. model[2].

Geological and stratigraphic context of the Huainan Basin

Palaeogeographic reconstructions situate the North China craton at the eastern tropical periphery of Rodinia[3]. The Huainan and Feishui groups constitute the earliest Neoproterozoic successions of the Huainan region, overlying the metamorphosed Mesoproterozoic Fengyang group[4]. The Huainan group starts with conglomerates and sandstones of the Caodian and Bagongshan Formations, conformably overlain by the ~700-800 m thick succession of the Liulaobei Formation. The Liulaobei Formation consists of calcareous marine mudstones intercalated with shales and siltstones, most of which were deposited below storm-wave base[5]. It hosts abundant acritarchs and macroscopic carbonaceous compressions[4,5]. The presence of Chuaria, Ellipsophysa and Tawuia assemblages in the Liulaobei Formation, and of characteristic early Neoproterozoic acritarchs (Trachyhystrichosphaera aimika) in the Liulaobei Formation, are consistent with a pre-Cryogenian age[4–6], also supported by Sr isotope data[7]. There is no published age for the Huainan Group, but the Liulaobei Formation is correlated to the <1069 ± 29 Ma Xinxing Formation[4,8,9].

The overlying Feishui group starts with sandstones of the Shouxian Formation, conformably overlain by argillaceous limestones of the Jiuliqiao Formation (~50 m thick), which is correlated to the Jiayuan and the Zhaowei Formations of the Huaibei Group. The lower Jiuliqiao Formation is composed of calcareous sandstone interbedded with carbonates; the upper Jiuliqiao Formation starts with argillaceous limestones characterized by intraclastic breccia and molar tooth structures[9]. The Jiuliqiao Formation sediments deposited below the storm-wave base, shallowing upwards, with the top of the succession containing abundant ripple marks. This succession yields acritarch assemblages and carbonaceous compressions similar to those present in the Liulaobei Formation[5]. Zircon U-Pb ages of >924.5 ± 9.5[10] for the Zhaowei Formation (Huaibei region), which correlates with the Jiuliqiao Formation[6], also point towards a Tonian age for the Feishui group. The Jiuliqiao Formation is conformably overlain by the ~250 m thick, dolomicritic Sidingshan Formation, which yields abundant intertidal stromatolitic structures.

Data quality checks on the P_{Fe} and P_{det} fractions

All geochemical data are presented in Table S1. Care is required when applying P speciation to ancient sedimentary rocks[11,12]. Notably, the potential recrystallization of authigenic CFA into well-crystalline P apatite[13] during burial diagenesis and metamorphism may mask original reactive P by increasing the apparent 'detrital' signal. Consequently, this would lead to an overestimation of the P_{det} pool to the detriment of P_{auth}, as observed for Cambrian phosphorite deposits[11]. The necessity of step V (Table S2) in our extraction protocol underlines the high crystallinity of highly recalcitrant apatite in these ancient sediments. However, in contrast to the study of Creveling et al. (ref. 11) where P_{det} represented on average 82% of the phosphorus budget, we note here that P_{auth} is a substantial P pool in the sediment (~29% of total P), and that there is no correlation between P_{auth} contents and P_{det}

contents (Fig. S1-A). Furthermore, there is a strong linear relationship between P_{det} and Al (as a proxy for the detrital input) within the Huainan group and the Feishui group (Fig. S1-B), which suggests that the measured P_{det} dominantly reflects the actual detrital P input, rather than post-depositional recrystallization. Hence, while a portion of the authigenic apatite pool may have recrystallized and been operationally extracted as P_{det}, these observations suggest that such a transfer was insignificant in terms of the dominant phase partitioning.

Thompson et al. (ref. 12) have recently proposed a modified protocol to ensure the full recovery of Fe-associated P (P_{Fe}) from crystalline hematite and magnetite in ancient rocks, and to evaluate the potential recrystallization of authigenic P into more crystalline minerals. In our samples, iron oxide-associated P constitutes the smallest P pool (Table S1), and P_{det} appears to approximate the detrital pool (Fig. S1-B). Nevertheless, we performed a comparison of the Thompson et al. protocol and the original Ruttenberg method[14], which revealed no significant differences (Fig. S2). The one-to-one correlation between the two protocols suggests that the Ruttenberg method used in this study was indeed appropriate, due to the very low P_{Fe} pool and limited recrystallization during burial.

Finally, the strong correlation between the total P digestion and the sum of each P extract (Fig. S3-A) suggests that individual P extractions successfully recovered the bulk P contents. We are therefore confident that our P speciation data are of high quality.

Extraction		P pool extracted
I	Na-dithionite extraction, citrate-buffered (pH 7.6; 8 h) $MgCl_2$ wash (2 h) H_2O wash (2x; 2 h)	P_{Fe}
II	Na-acetate extraction (pH 4; 6 h) $MgCl_2$ wash (2x; 2 h) H_2O wash (as required; 2 h)	P_{auth}
III	HCl extraction (1 M, 16 h)	$P_{det, 1}$
IV	Ashing at 550ºC HCl extraction (1 M, 16 h, 24 h)	P_{org}
V	HNO_3-HF-$HClO_4$-H_3BO_3-HCl extraction on residue	$P_{det, 2}$
VI	HNO_3-HF-$HClO_4$-H_3BO_3-HCl extraction on bulk sediment	P_{tot}

Replicates	P_{Fe} ppm	P_{auth} ppm	P_{det} ppm	P_{org} ppm	P_{tot} ppm
A	8	97	268	10	383
B	13	92	289	8	404
C	10	100	267	8	344
D	12	94	281	8	390
E	12	107	285	8	415
Mean	11	98	278	8	387
SD	2	6	10	1	27
RSD%	16	6	4	9	7

Table S2. Upper part: SEDEX extraction steps and targeted P pools, modified for ancient sedimentary rocks. Lower part: Replicate analysis of [P] concentrations obtained for each targeted P pool.

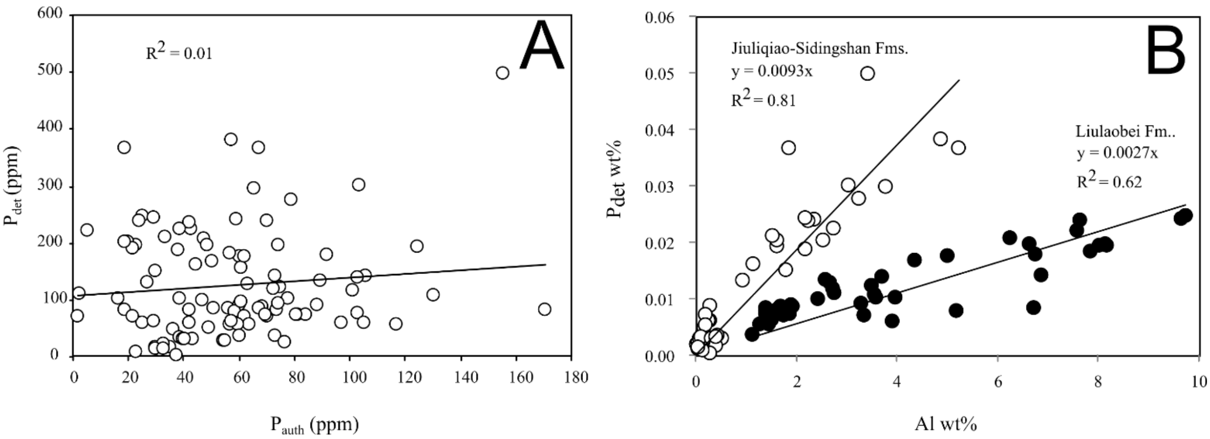

Figure S1. Assessment of potential pool transfer of P_{auth} to P_{det}. The lack of correlation between P_{det} and P_{auth} is not supportive of a genetic relationship between both pools (A). The correlations between P_{det} and Al contents in the different formations (B) support that P_{det} is inherited from the detrital input.

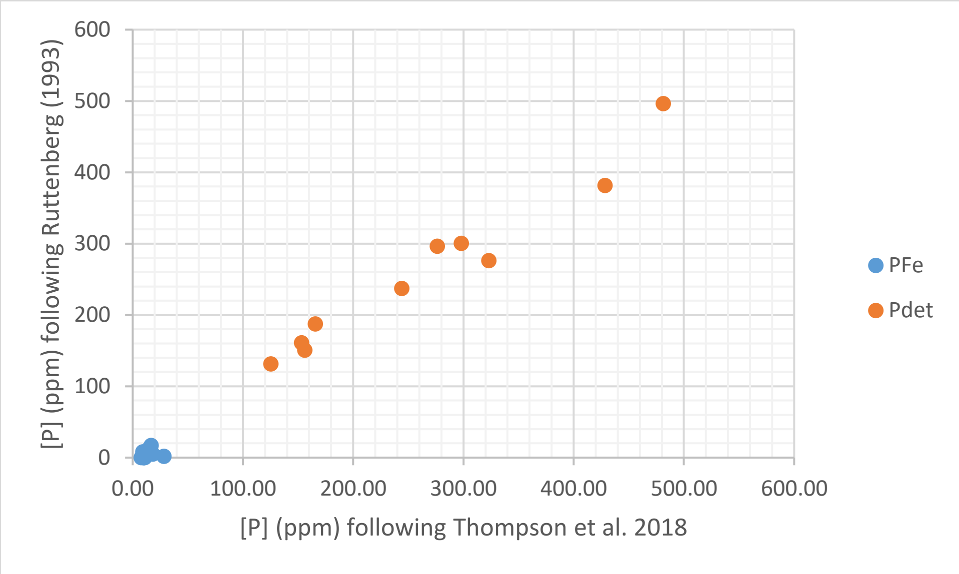

Figure S2. P_{Fe} and P_{det} plots comparing the Ruttenberg and the Thompson methods.

C isotope quality checks

Several lines of evidence suggest that the carbon isotope signatures ($\delta^{13}C$) in our samples are pristine and not significantly altered by secondary overprinting, including i) the lack of correlation between the carbon isotope composition of carbonates ($\delta^{13}C_{carb}$) and coeval oxygen isotope values ($\delta^{18}O_{carb}$; ref. 15), and ii) Mn/Sr ratios <10 (ref. 16), as shown by Fig. S3. Two samples from one locality (samples referred to as "Mli"), for which Mn/Sr ranges from ~0.5 to ~13.6, exceed this threshold, suggesting that these two samples may have been affected by secondary processes.

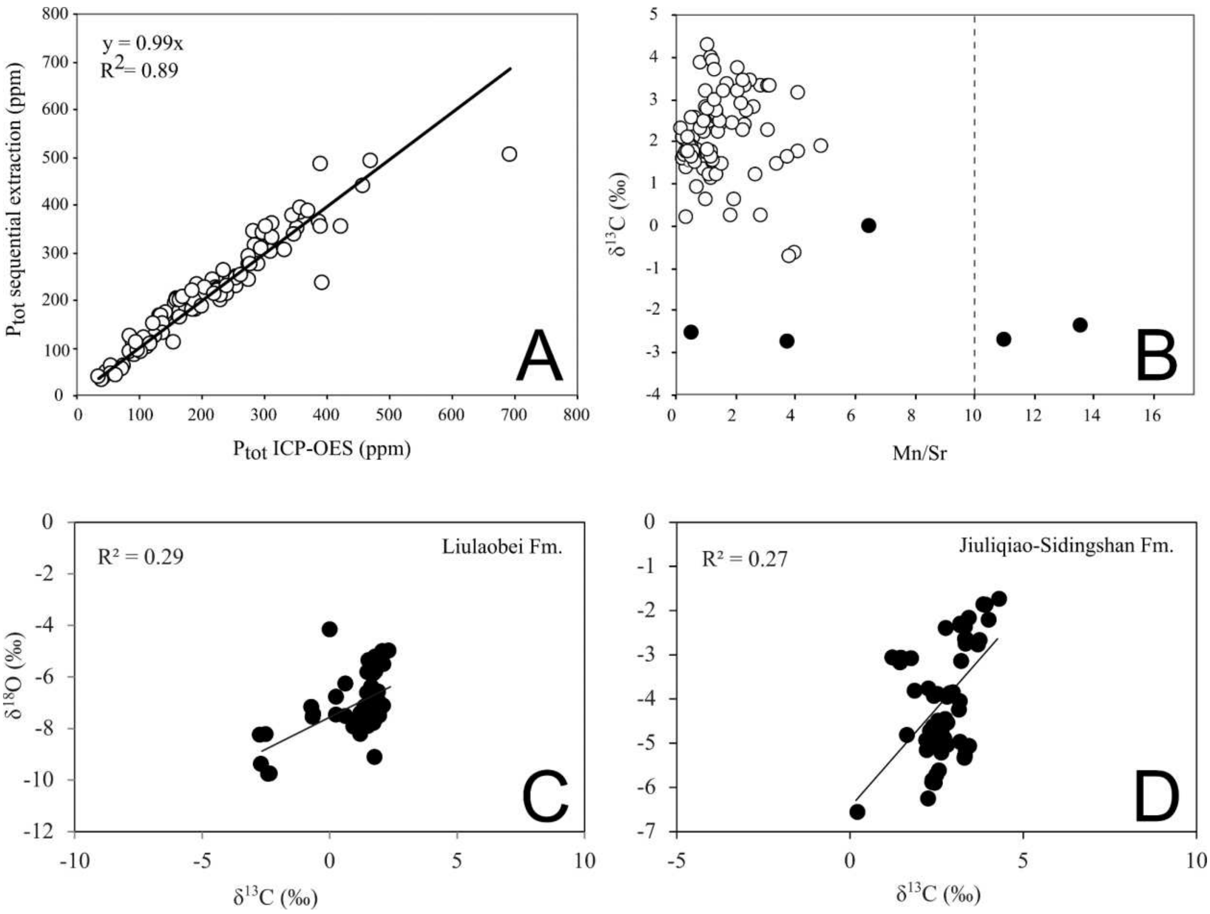

Figure S3. (A) Phosphorus extractions quality check based on the correlation between total P digestion and the sum of each P extract. (B) Assessment of potential secondary alterations of C isotope during diagenesis based on the relative mobility of Mn and Sr. The black circles represent the “Mli” sample outcrop which is likely to have experienced diagenetic overprinting. (C-D) Assessment of potential C and O isotope resetting from meteoric water and/or burial diagenesis for the Liulaobei Fm. and the Jiuliqiao-Sidingshan Fm.

Previously published Fe speciation data for the Huainan Basin

Fe speciation data for the Huainan basin[17] are illustrated by Fig. S4. The persistence of ferruginous water column conditions in the region (and elsewhere throughout the early Neoproterozoic) has been established previously[17], using the well-established Fe speciation method. The method targets operationally defined Fe pools, including carbonate associated-Fe (Fe_{Carb}), ferric oxides-Fe (Fe_{Ox}), magnetite-Fe (Fe_{Mag}), sulphide-Fe (Fe_{Py}) and total Fe

(Fe_T). Water column conditions are determined by quantifying the proportion of biogeochemically highly reactive Fe (Fe_{HR}, defined as the sum of Fe_{Carb} + Fe_{Ox} + Fe_{Mag} + Fe_{Py}) relative to Fe_T.. Anoxic water columns promote Fe_{HR} enrichments in the underlying sediments, and anoxic deposition is typically characterized by sedimentary Fe_{HR}/Fe_T ratios >0.38 (ref. 18). By contrast, sediments deposited under oxic water column conditions lack Fe_{HR} enrichments and are characterised by low Fe_{HR}/Fe_T ratios (<0.22; ref. 18). For anoxic samples, ferruginous conditions are distinguished from euxinic settings by quantifying the extent of sulphidation of the highly reactive pool (Fe_{py}/Fe_{HR}). Fe_{py}/Fe_{HR} >0.7 is characteristic of euxinic deposition, whereas Fe_{py}/Fe_{HR} <0.7 indicates deposition under ferruginous conditions[18]. The speciation of highly reactive Fe is dominantly represented by carbonate associated Fe and ferric oxides, with minor contributions from magnetite and sulphides (Fig. S4).

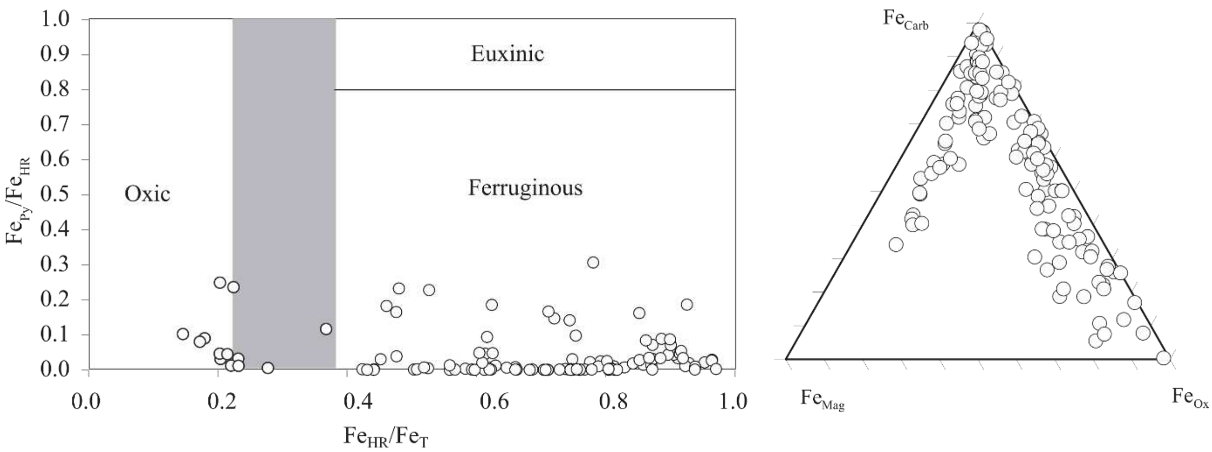

Figure S4. Iron speciation in the Huainan basin, after ref. 17. Highly reactive iron phases include carbonate associated-Fe (Fe_{Carb}), ferric oxides-Fe (Fe_{Ox}), magnetite-Fe (Fe_{Mag}) and sulphide-Fe (Fe_{Py}). Fe_T stands for total Fe.

TOC contents through time

The very low TOC contents observed throughout the Huainan basin succession are in agreement with other early Neoproterozoic shales (e.g., refs. 17,19,20). This contrasts with the still limited dataset of higher TOC contents characterizing the preceding Mesoproterozoic (e.g., refs. 1,21–25) (Fig. S5). We suggest that in the early Neoproterozoic, effective P removal under widespread ferruginous conditions and fixation in sediments exerted a negative feedback on primary production (hence decreasing the flux of organic C burial). By contrast, large expanses of mid-depth euxina in the preceding Mesoproterozoic likely promoted intense P recycling to the water column (Fig. 4), with a positive feedback on primary production, and enhanced fluxes of organic C burial.

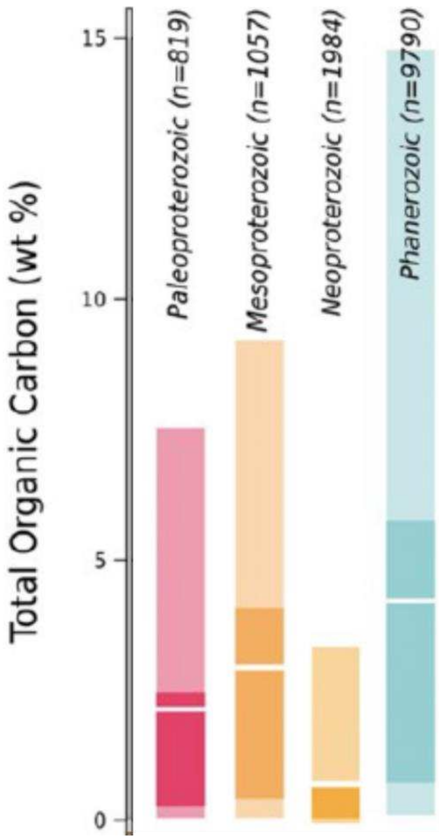

Figure S5. Summary compilation of total organic carbon through the Proterozoic and the Phanerozoic, modified after ref. 1. Horizontal white lines represent the medians and the boxes represent the first and third quartiles.

Compilation of P speciation and C/P data for the Phanerozoic (Table S3)

Cambrian P speciation and C/P data consist of >100 samples from recrystallized, phosphate-rich carbonates deposited under ferruginous conditions[11]. Devonian data consist of bioturbated and laminated shales (n = 76) from the Camp Run Member[26]. Cretaceous data include shales (n = 306) deposited under ferruginous and euxinic conditions during Ocean Anoxic Event 2 (refs. 27,28) and under ferruginous conditions during Ocean Anoxic Event 3 (ref. 29). Numerous ODP sediment samples spanning the last 65 million years (Ma) and over various redox depositional conditions were also compiled, including 297 samples[30] from sites in the California Current region (ODP leg 167, sites 1010, 1011, 1012, 1014, 1016, and 1021), in the Benguela Current region (ODP leg 175, sites 1082, 1084, and 1085), and on Blake Nose in the western Atlantic (ODP leg 171B, sites 1050 and 1052), and 237 samples from the Western and Eastern equatorial Pacific[31]. Recent Phanerozoic sediments deposited under oxic and euxinic bottom waters were compiled for the California margin, the San Clemente Basin, the Eastern North Pacific, the Santa Monica Basin and the Washington continental margin[32]. Additional samples are from the Baltic Proper[33] and eastern Mediterranean sapropels[34]. Sediments deposited under oxic and oligotrophic conditions are from the Bothnian Sea[35,36] and from subtropical gyres[37].

Sample	Bottom water redox condition	P_{exch}/P_{tot}	P_{Fe}/P_{tot}	P_{auth}/P_{tot}	P_{det}/P_{tot}	P_{org}/P_{tot}	C_{org}/P_{org}	C_{org}/P_{reac}	C_{org}/P_{tot}	Reference
Cambrian carbonates	ferruginous		0	8	92	0			<100	*Creveling et al., 2012*
Devonian shales	oxic							150		*Ingall et al., 1993*
Devonian shales	'anoxic'							3900		*Ingall et al., 1993*
OAE 2	'anoxic'		5	← 89 →		4		>500		*Mort et al., 2007*
OAE 2	ferruginous/euxinic								>600	*Poulton et al., 2015*
OAE 3	ferruginous		13	34	2	1	>1000	<50	<50	*Marz et al., 2008*
This study	ferruginous		5	29	58	9	135	24	8	*This study*
Bothnian (oligotrophic)	oxic	0	58	23	6	13	261	37	35	*Egger et al., 2015*
Bothnian (oligotrophic)	oxic	1	51	18	7	16	326	60	56	*Slomp et al., 2013*
East Mediterranean	oxic		28	35	12	23	210	50	44	*Slomp et al., 2004*
	anoxic sapropel						427	109	95	*Slomp et al., 2004*
Baltic Proper	oxic/euxinic	2	12	13	13	59	249	148	129	*Mort et al., 2010*
Various ODP	mainly oxic		9	82	12	8	970	89	71	*Anderson et al., 2001*
Equatorial Pacific	mainly oxic	5	10	81	1	5				*Filipelli and Delaney, 1996*
Various modern sites	oxic/'anoxic'								<600	*Ingall and Jahnke, 1997*
Subtropical gyres	oligotrophic						<600			*Teng et al., 2014*

Table S3. Compilation of C/P ratios and P speciation data for Phanerozoic sediments, compared to our study.

Geological and redox context of the Taoudeni Basin and the Animikie Basin

Our study was augmented by euxinic shales from the ~1.1 Ga Atar/El Mreiti Group at the north-western edge of the Taoudeni Basin (Mauritania). The sediments deposited under a range of relatively shallow environments, from fluvial and shallow marine, to more proximal settings (below wave base)[38]. Drill core samples from low metamorphic grade black shales of the ~1.8 Ga Animikie group, Superior Province, North America, were also analysed. The samples have been fully described elsewhere[12,22]. We specifically selected sediments that deposited under persistently euxinic water columns, in order to draw a comparison between P recycling regimes under both dominantly ferruginous (Huainan Basin) and euxinic settings.

Water column redox chemistry was determined by the Fe speciation method[39], and the samples analysed all display Fe_{HR}/Fe_{T} >0.38 and Fe_{Py}/Fe_{HR} >0.7 (ref. 18). P speciation was performed using the same protocols as for the Huainan Basin, and we focussed on the total, reactive and organic-bound fractions of P (Table S1).

Model assumptions

The observation that the Great Oxidation Event (GOE) was never reversed places an important constraint on Earth's surface redox balance[2]: there must have consistently been a net source of O_2 in excess of the input flux of reduced gases, which oxidise rapidly and completely.

We argue the sulphur cycle was not a major contributor to maintaining this redox balance through much of the Proterozoic. Given widely-recognized complete oxidative weathering of pyrite after the GOE (i.e. the disappearance of detrital pyrite), subsequent reduction of SO_4 and reburial as pyrite has no net effect on Earth's surface redox balance. In principle, gypsum weathering followed by pyrite burial could provide a net source of O_2. However, this necessarily drains the gypsum sedimentary reservoir which anyway must have been small up to ~1 Ga, because of limited evaporite deposition beforehand linked to low [SO_4] and limited evaporite basin areas[17]. Instead, a large increase in SO_4 deposition in gypsum evaporites around ~1 Ga associated with the low-latitude amalgamation of Rodinia[17], more likely represented a net O_2 sink (assuming, plausibly, that it exceeded gypsum weathering).

Therefore, the key controller of Earth's surface redox balance and atmospheric oxygen levels through much of the Proterozoic, as today, was the carbon cycle. The oxidative weathering of ancient organic matter (kerogen) after the GOE was kinetically-limited and incomplete[2]. Hence burial of new organic carbon in excess of this oxidative weathering of ancient organic carbon represented a key net oxygen source. In the limit of declining O_2, which tends to shut down ancient kerogen oxidation, the burial flux of new organic carbon must have exceeded the input flux of reduced gases to maintain an oxidizing atmosphere, a present-day minimum estimate for which is $\sim 1.25 \times 10^{12}$ mol O_2 eq yr^{-1} (ref. 2). The main text gives corresponding estimates of phosphorus and organic carbon burial fluxes, extrapolating from maximum total P and TOC in our sample location shales, and an assumed pre-anthropogenic sediment erosion rate. The resulting reactive P weathering/burial flux estimate is comparable to today and the estimated C_{org} burial flux of $<1.75 \times 10^{12}$ mol C yr^{-1} is sufficient to maintain an oxidizing atmosphere.

Two other recent models give comparable or larger estimates of the organic carbon burial flux consistent with maintaining Proterozoic Earth surface redox balance with an oxidizing atmosphere. Ozaki et al. (ref. 40), under their "Low O_2" (0.0001-0.01 PAL) assumption, estimate a median 1.1×10^{12} mol O_2 eq yr^{-1} organic carbon burial, which increases to 1.64×10^{12} mol O_2 eq yr^{-1} under their "High O_2" (0.01-0.1 PAL) assumption (consistent with our model). We note that their "Low O_2" scenario assumes incomplete oxidative weathering of pyrite, which seems inconsistent with the disappearance of detrital pyrite after the GOE. Yet it already demands a large (non-S) reductant input to stop O_2 rising towards what we view as the more plausible levels of their "High O_2" scenario. Even that "High O_2" scenario has a large excess of pyrite burial over pyrite weathering and assumed reduced gaseous/hydrothermal S input, demanding a significant net S input from gypsum weathering and significant growth of the sedimentary pyrite reservoir at the expense of what has to be a significant gypsum reservoir. Whether or not an initial gypsum reservoir ~25% of present at 1.8 Ga can be justified, such net transfer of S could not be sustained over Proterozoic timescales – we estimate the gypsum reservoir would be drained in ~200 Myr.

Laakso and Schrag (ref. 41) in their "Low-O_2" Proterozoic model state estimate a much higher 4.3×10^{12} mol O_2 eq yr^{-1} "organic burial" close to their assumed modern value (4.8×10^{12} mol O_2 eq yr^{-1}). They show a Proterozoic sulphur cycle dominated by gypsum burial, which given complete pyrite oxidation, makes the S cycle a massive net O_2 sink. This explains the need for a massive organic burial flux, but this is not supported by with the S isotope record, which clearly indicates a dominance of pyrite burial through the Proterozoic[42].

Supplementary references:

1. Sperling, E. A. & Stockey, R. G. The Temporal and Environmental Context of Early Animal Evolution: Considering All the Ingredients of an "Explosion". Integr. Comp. Biol. **58**, 605–622 (2018).
2. Daines, S. J., Mills, B. J. & Lenton, T. M. Atmospheric oxygen regulation at low Proterozoic levels by incomplete oxidative weathering of sedimentary organic carbon. Nat. Commun. **8**, 14379 (2017).

3. Li, Z. X. et al. Assembly, configuration, and break-up history of Rodinia: A synthesis. Test. Rodinia Hypothesis Rec. Its Build. Blocks **160**, 179–210 (2008).
4. Dong, L. et al. Restudy of the worm-like carbonaceous compression fossils Protoarenicola, Pararenicola, and Sinosabellidites from early Neoproterozoic successions in North China. Dawn Anim. Life Evol. Palaeoecol. Patterns Neoproterozoic-Cambr. Anim. Foss. Rec. Dawn Anim. Life Evol. Palaeoecol. Patterns Neoproterozoic-Cambr. Anim. Foss. Rec. Geol. Soc. Am. Annu. Meet. **258**, 138–161 (2008).
5. Tang, Q. et al. Organic-walled microfossils from the early Neoproterozoic Liulaobei Formation in the Huainan region of North China and their biostratigraphic significance. Precambrian Res. **236**, 157–181 (2013).
6. Xiao, S. et al. Biostratigraphic and chemostratigraphic constraints on the age of early Neoproterozoic carbonate successions in North China. Precambrian Res. (2014) doi:10.1016/j.precamres.2014.03.004.
7. Yang, J., Zheng, W., Wang, Z. & Tao, X. Age determining of the Upper Precambrian system of northern Jiangsu-Anhui by using Sr and C isotopes. J. Stratigr. **25**, 44–47 (2001).
8. Yang, D.-B. et al. U–Pb ages and Hf isotope data from detrital zircons in the Neoproterozoic sandstones of northern Jiangsu and southern Liaoning Provinces, China: Implications for the Late Precambrian evolution of the southeastern North China Craton. Precambrian Res. **216–219**, 162–176 (2012).
9. Wang, G. et al. Research on the upper Precambrian of northern Jiangsu and Anhui Provinces. Hefei Anhui Press Sci. Technol. (1984).
10. Fu, X. et al. New paleomagnetic results from the Huaibei Group and Neoproterozoic mafic sills in the North China Craton and their paleogeographic implications. Precambrian Res. **269**, 90–106 (2015).

11. Creveling, J. R. et al. Phosphorus sources for phosphatic Cambrian carbonates. Geol. Soc. Am. Bull. **126**, 145–163 (2014).

12. Thompson, J. et al. Development of a modified SEDEX phosphorus speciation method for ancient rocks and modern iron-rich sediments. Chem. Geol. **524**, 383–393 (2019).

13. Shemesh, A. Crystallinity and diagenesis of sedimentary apatites. Geochim. Cosmochim. Acta **54**, 2433–2438 (1990).

14. Ruttenberg, K. C. Development of a sequential extraction method for different forms of phosphorus in marine sediments. Limnol. Oceanogr. **37**, 1460–1482 (1992).

15. Loyd, S. J. et al. Sustained low marine sulfate concentrations from the Neoproterozoic to the Cambrian: Insights from carbonates of northwestern Mexico and eastern California. Earth Planet. Sci. Lett. **339**, 79–94 (2012).

16. Kaufman, A. J. & Knoll, A. H. Neoproterozoic variations in the C-isotopic composition of seawater: stratigraphic and biogeochemical implications. Precambrian Res. **73**, 27–49 (1995).

17. Guilbaud, R., Poulton, S. W., Butterfield, N. J., Zhu, M. & Shields-Zhou, G. A. A global transition to ferruginous conditions in the early Neoproterozoic oceans. Nat. Geosci. **8**, 466–470 (2015).

18. Poulton, S. W. & Canfield, D. E. Ferruginous Conditions: A Dominant Feature of the Ocean through Earth's History. Elements **7**, 107–112 (2011).

19. Dahl, T. W. et al. Molybdenum evidence for expansive sulfidic water masses in~ 750Ma oceans. Earth Planet. Sci. Lett. **311**, 264–274 (2011).

20. Sperling, E. A., Halverson, G. P., Knoll, A. H., Macdonald, F. A. & Johnston, D. T. A basin redox transect at the dawn of animal life. Earth Planet. Sci. Lett. (2013).

21. Planavsky, N. J. et al. Widespread iron-rich conditions in the mid-Proterozoic ocean. Nature **477**, 448–451 (2011).

22. Poulton, S. W., Fralick, P. W. & Canfield, D. E. Spatial variability in oceanic redox structure 1.8 billion years ago. Nat. Geosci **3**, 486–490 (2010).

23. Geboy, N. J. et al. Re–Os age constraints and new observations of Proterozoic glacial deposits in the Vazante Group, Brazil. Precambrian Res. **238**, 199–213 (2013).

24. Gilleaudeau, G. J. & Kah, L. C. Oceanic molybdenum drawdown by epeiric sea expansion in the Mesoproterozoic. Chem. Geol. **356**, 21–37 (2013).

25. Shen, Y., Knoll, A. H. & Walter, M. R. Evidence for low sulphate and anoxia in a mid-Proterozoic marine basin. Nature **423**, 632–635 (2003).

26. Ingall, E. D., Bustin, R. & Van Cappellen, P. Influence of water column anoxia on the burial and preservation of carbon and phosphorus in marine shales. Geochim. Cosmochim. Acta **57**, 303–316 (1993).

27. Mort, H. P. et al. Phosphorus and the roles of productivity and nutrient recycling during oceanic anoxic event 2. Geology **35**, 483–486 (2007).

28. Poulton, S. W. et al. A continental-weathering control on orbitally driven redox-nutrient cycling during Cretaceous Oceanic Anoxic Event 2. Geology **43**, 963–966 (2015).

29. März, C. et al. Redox sensitivity of P cycling during marine black shale formation: dynamics of sulfidic and anoxic, non-sulfidic bottom waters. Geochim. Cosmochim. Acta **72**, 3703–3717 (2008).

30. Anderson, L., Delaney, M. & Faul, K. Carbon to phosphorus ratios in sediments: Implications for nutrient cycling. Glob. Biogeochem. Cycles **15**, 65–79 (2001).

31. Filippelli, G. M. & Delaney, M. L. Phosphorus geochemistry of equatorial Pacific sediments. Geochim. Cosmochim. Acta **60**, 1479–1495 (1996).

32. Ingall, E. & Jahnke, R. Influence of water-column anoxia on the elemental fractionation of carbon and phosphorus during sediment diagenesis. Phosphorus Cycl. Sediment. Mar. Freshw. Syst. **139**, 219–229 (1997).

33. Mort, H. P., Slomp, C. P., Gustafsson, B. G. & Andersen, T. J. Phosphorus recycling and burial in Baltic Sea sediments with contrasting redox conditions. Geochim. Cosmochim. Acta **74**, 1350–1362 (2010).

34. Slomp, C. P., Thomson, J. & de Lange, G. J. Controls on phosphorus regeneration and burial during formation of eastern Mediterranean sapropels. Mar. Geol. **203**, 141–159 (2004).

35. Egger, M., Jilbert, T., Behrends, T., Rivard, C. & Slomp, C. P. Vivianite is a major sink for phosphorus in methanogenic coastal surface sediments. Geochim. Cosmochim. Acta **169**, 217–235 (2015).

36. Slomp, C. P. et al. Coupled dynamics of iron and phosphorus in sediments of an oligotrophic coastal basin and the impact of anaerobic oxidation of methane. PloS One **8**, e62386 (2013).

37. Teng, Y.-C., Primeau, F. W., Moore, J. K., Lomas, M. W. & Martiny, A. C. Global-scale variations of the ratios of carbon to phosphorus in exported marine organic matter. Nat. Geosci. **7**, 895 (2014).

38. Gilleaudeau, G. J. & Kah, L. C. Heterogeneous redox conditions and a shallow chemocline in the Mesoproterozoic ocean: evidence from carbon–sulfur–iron relationships. Precambrian Res. **257**, 94–108 (2015).

39. Poulton, S. W. & Canfield, D. E. Development of a sequential extraction procedure for iron: implications for iron partitioning in continentally derived particulates. Chem. Geol. **214**, 209–221 (2005).

40. Ozaki, K., Reinhard, C. T. & Tajika, E. A sluggish mid-Proterozoic biosphere and its effect on Earth's redox balance. Geobiology **17**, 3–11 (2019).

41. Laakso, T. A. & Schrag, D. A theory of atmospheric oxygen. Geobiology **15**, 366–384 (2017).

42. Canfield, D. E. The evolution of the Earth surface sulfur reservoir. Am. J. Sci. **304**, 839–861 (2004).